polymers

MDPI

Article

Influence of Nano Titanium Dioxide and Clove Oil on Chitosan–Starch Film Characteristics

Wei Li [1], Kewang Zheng [1,*], Hujian Chen [1], Shirong Feng [1], Wei Wang [1] and Caiqin Qin [1,2,*]

[1] School of Chemistry and Materials Science, Hubei Engineering University, Xiaogan 432000, China
[2] Key Laboratory of Biological Resources and Environmental Biotechnology, Wuhan University, Wuhan 430000, China
* Correspondence: kewang@hbeu.edu.cn (K.Z.); qincq@hbeu.edu.cn (C.Q.); Tel.: +86-07122345464 (K.Z.); +86-07122345697 (C.Q.)

Received: 31 July 2019; Accepted: 27 August 2019; Published: 29 August 2019

Abstract: The combined effects of nano titanium dioxide (TiO_2-N) and clove oil (CO) on the physico-chemical, biological and structural properties of chitosan (CH)/starch (ST) films were investigated by using a solvent casting method. Results indicated that the incorporation of TiO_2-N could improve the compactness of the film, increase the tensile strength (TS) and antioxidant activity, and decrease the water vapour permeability (WVP). As may be expected, the incorporation of CO into the film matrix decreased TS but increased the hydrophobicity as well as water vapour barrier antimicrobial and antioxidant properties. Fourier-transform infrared spectroscopy (FTIR) data supported intermolecular interactions between TiO_2-N, CO and the film matrix. Use of a scanning electron microscope (SEM) showed that TiO_2-N and CO were well dispersed and emulsified in the film network. Thermogravimetric (TG) and derivative thermogravimetric (DTG) curves demonstrated that TiO_2-N and CO were well embedded in the film matrix, hence this blend film system could provide new formulation options for food packaging materials in the future.

Keywords: chitosan; starch; nano titanium dioxide; clove essential oil; edible film

1. Introduction

In the past decades, the use of synthetic packaging materials, such as polyethylene terephthalate (PET), polyethylene (PE) and polypropylene (PP), has become increasingly popular worldwide. Despite synthetic packaging materials having good physico-chemical properties and a low cost, they have caused significant environmental pollution due to their non-biodegradable and unrecyclable nature. Besides, some plastic additives, such as bisphenol A (BPA), dioctyl phthalate (DOP) and dibutyl phthalate (DBP), readily migrate from packaging films to food, thus leading to harm to human health. Therefore, the development of eco-friendly packaging materials is necessary [1,2]. Eco-friendly packaging materials usually include biodegradable films and coatings, which are based on bio-polymers (carbohydrates, proteins and lipids), additives and functional ingredients [3,4]. Among bio-polymers, chitosan and starch have been the focus of current research due to their biodegradability, good film-forming capacity, edibility and natural availability [5–9].

Chitosan, the product of chitin deacetylation, is a natural biopolymer which has been widely applied in the manufacturing of biodegradable films or coatings for its biocompatibility, biodegradation and good film-forming ability [10,11]. However, chitosan film has poor mechanical properties and little water resistance, which has limited its application [11]. Therefore, some strategies have been applied to modify them. For example, the use of a natural biopolymer such as starch, incorporated into chitosan film, is one of the most widespread and cheap ways used to improve film properties [12–14]. However, poor antioxidant, antimicrobial and water vapour barrier properties were the main disadvantages of

chitosan–starch-based films. To enhance the performance thereof, several strategies have been adopted, such as incorporating inorganic nanoparticles and essential oils into the chitosan–starch-based matrix due to essential oils or inorganic nanoparticles possessing good barrier, hydrophobic, mechanical, thermal, antimicrobial and anti-oxidation properties [15–20].

Incorporation of inorganic nano-fillers, such as zinc oxide, silver, silica and clay into food packaging has been proven to enhance the physico-chemical and other properties of biodegradable films compared to the neat matrices [21–23]. Titanium dioxide (TiO_2) as functional filler has been widely applied in medicines, foodstuffs and feed processing due to its non-toxicity, security, high stability and antibacterial properties [24]. It was reported that the addition of TiO_2-N into food packaging materials could provide food prevention against growth of microorganisms [25,26]. However, TiO_2-N offers poor anti-oxidation activity which is its main disadvantage in practice (oxidation is one of the important causes of food spoilage), whereas many plant essential oils have been proved to have excellent antioxidant and antibacterial activities [27,28]. Moreover, the essential oils were usually incorporated into the bio-polymer matrix to enhance its water-barrier properties. Clove oil (CO) is extracted from lilac and its main constituent is eugenol. CO has been reported to have excellent antimicrobial and anti-oxidation activities [29] and has received FDA approval for use within food and medicine. Recently, inorganic nanoparticles and essential oil have been proved to improve the physico-chemical and biological properties of edible film [30]. Wu et al. [31] developed an edible film based on a soy protein isolate, cinnamaldehyde and zinc oxide nanosheet. Their research showed that zinc oxide and cinnamaldehyde have a synergistic effect on the physico-chemical properties and antifungal activity of edible film. Wu et al. [32] found that a chitosan coating containing both laurel essential oil and nanosilver had better antioxidant properties than a regular coating, laurel essential oil coating and nanosilver coating.

There are, however, few reports of the application of TiO_2-N and CO on edible films. Considering the excellent antioxidant and antibacterial activities of CO and TiO_2-N, the aim of this work was to obtain an active film based on chitosan, starch, TiO_2-N and CO, and investigate the influences of TiO_2-N and CO contents on the physico-chemical, morphological, biological and structures properties of the film.

2. Materials and Methods

2.1. Materials

Chitosan (CH, $M_v = 1.98 \times 10^5$ g/mol, degree of deacetylation ≥ 82%) was supplied by Shandong AK Biotech Co. Ltd. (Qingdao, China). Starch (ST) was supplied by National Starch Co. Ltd. (Shanghai, China). Clove oil (CO) as a guarantee reagent, the TiO_2-N (rutile, particle size = 40 nm, and purity ≥ 99.8%) and other reagents were all purchased from Aladdin Biochemical Co. Ltd. (Shanghai, China).

2.2. Film Preparation

CH solution was obtained by dissolving 1.5 g/100 mL CH in 1 mL/100 mL acetic acid with constant agitation overnight at room temperature. ST was dispersed in water to get 1.5 g/100 mL suspension, which was heated to 90 °C and held for 35 min under stirring to allow gelatinisation. The CH–ST solution was obtained by addition of 100 mL of CH solution to an equal volume of ST solution, then 18% *w*/*w* (based on CH and ST) glycerol was added as the plasticiser. Thereafter, the CH–ST solution was cooled to around 45 °C before adding TiO_2-N and CO. To achieve better dispersion of TiO_2-N and emulsification of CO, different concentrations (1%, 3%, 5% and 7% *w*/*w*) of TiO_2-N was dispersed in 20 mL of distilled water and then ultrasonicated for 10 min. Different concentrations (3%, 6%, 9% and 12% *w*/*w*) of CO could be first mixed with 10% (*w*/*w*, total CO) Tween 80 and then the mixture was dissolved in 3 mL ethyl alcohol.

The film-forming dispersion (FFD) was prepared by mixing the CH–ST solution, TiO_2-N suspension and CO emulsion. Then, the film forming solution was homogenised at 40 °C at 9000 rpm in a homogeniser for 5 min (FJ-300SH, Shanghai Specimen, Shanghai, China), filtered through cheesecloth and vacuumed. Finally, the FFD was poured into plastic discs (diameter of 90 mm) and dried at 38 °C and a relative humidity (RH) of 53% (using a saturated sodium bromide solution) to obtain the films. Before testing, all samples were stored at 25 °C and 57% RH for at least 48 h. A control film specimen was obtained in a similar manner but without any TiO_2-N or CO.

2.3. Determination of Film Structure

The FTIR spectra of the sample were recorded using a Bruker Vertex 80 spectrometer equipped with an ATR accessory from 700 to 4000 cm^{-1}. The thermal stability of the sample was recorded in a differential thermal analyser (STA6000, Perkins Elmer, Norwalk, CT, USA) under a nitrogen atmosphere, using a heating rate of 10 °C/min and the programmed temperature ranged from 30 °C to 800 °C. The morphology of the sample was recorded using a video recorder (D7500, Nikon, Tokyo, Japan). Microstructural analysis of the cross-sections of samples was facilitated by use of an SEM (EVO, Zeiss, Heidenheim, Germany) with an accelerating voltage of 5 kV. Before testing, the film was gold coated.

2.4. Physico-Chemical Properties

After using a digital micrometer (WHX, Xinzhenwei, Shanghai, China) to record the sample thickness at nine random positions, mechanical testing was performed through the method described by Zheng et al. [27]. Samples were cut into rectangular pieces (10 mm × 70 mm); the initial grip separation was 30 mm, and the crosshead displacement rate was 20 mm/min.

The moisture content (MC) of each specimen was measured by thermogravimetric analysis (TGA) [33]. The heating rate applied to the film was 5 °C/min and the programmed temperature ranged from 30 °C to 150 °C. The water contact angle was measured by a static contact-angle meter (JC2000, Powereach, Shanghai, China). Film was put on the sample stage, and the contact angle was measured immediately after dropping 1 μL distilled water on the sample surface [34].

The WVP of samples was determined by using a published method with some modifications [17]: 10 g of oven-dried calcium chloride ($CaCl_2$) was poured into a permeation cup (diameter, 50 mm), and each sample (65 mm diameter) was sealed on the cup. Then the permeation cup was put in a box at a temperature of 25 °C at 78% RH and weighed every 8 h for 4 d.

Optical properties of samples were evaluated by the methods of colour difference and opacity. Opacity was measured using an UV-Vis spectrophotometer (UV1800, Jinghua, Shanghai, China) with an incident wavelength of 600 nm. The optical properties were calculated as follows:

$$O = Abs_{600}/L \quad (1)$$

where L and Abs_{600} are the film thickness (mm) and absorbance at 600 nm, respectively.

The colour difference was measured by a colorimeter (WSC-C, KingKo, Shanghai, China). The values of L^*, a^* and b^* represent the intensity of black–white, red–green, and yellow–blue light, respectively. The whiteness index (WI) of the film was calculated as follows:

$$WI = 100 - \sqrt{(100 - L^*)^2 + a^{*2} + b^{*2}} \quad (2)$$

2.5. Biological Properties

The antibacterial activity of samples was assessed using the agar diffusion method: 1 mL (10^8 to 10^9 CFU/mL) of microorganic liquid (*Escherichia coli or Staphylococcus aureus*) was seeded with 15 mL of agar medium. Then, samples (diameter, 6 mm) were placed on the agar plate surface, and the plate was stored at 37 °C for 24 h. The area of the inhibition zone was calculated and subtracted from the sample disk area, and this difference in area was used as the inhibition zone.

The antioxidant activity of sample was performed by the 2, 2-Diphenyl-1-pikryl-hydrazyl (DPPH) scavenging assay and 2, 2′-azino-bis(3-ethylbenzothiazoline-6-sulfonic acid (ABTS) scavenging assay. Before the test, the film (0.6 g) was soaked in 30 mL distilled water and stood for 12 h at 25 °C to obtain the film extract solution. A total of 2 mL of the DPPH methanol solution (1 mM) was mixed with 1 mL of the film extract solution, and the mixture was well shaken and put in a dark chamber at 25 to 30 °C for 1 h. The mixture was measured with a UV spectrophotometer (UV1800, Jinghua, Shanghai, China) with an incident wavelength of 517 nm. The ABTS radical scavenging activity of film was evaluated using the method of Zheng et al. with some modification [35]. Before the test, 5 mL ABTS solution (7.4 mM) and 88 µL $K_2S_2O_8$ solution (2.6 mM) were mixed, and the mixture was stored for 12 h. A total of 2 mL ABTS working solution was mixed with 0.1 mL of film extract solution, and the absorbance was measured at 734 nm after standing for 10 min in a dark chamber. The DPPH and ABTS scavenging activities of samples were determined as follows:

$$\text{Activity } (\%) = \frac{(A_0 - A_s)}{A_0} \times 100 \quad (3)$$

where A_0 and A_s were the absorbances of the control solution and tested sample solution, respectively.

2.6. Statistical Analysis

Data analysis was done through SPSS software (SPSS 16.0.2, Palo Alto, CA, USA). Statistical significance of differences in means was obtained by ANOVA and the Duncan's multiple range tests at $p < 0.05$. Data were presented as mean ± standard deviation.

3. Results and Discussion

3.1. Characterization of Film

3.1.1. FTIR Spectroscopy

The IR spectra of different films are shown in Figure 1. For control specimens, a strong broad peak located at 3420 cm^{-1} was caused by the stretching vibration of free O–H, which was probably due to the presence of hydroxyl groups [36]. The bands at 1640 cm^{-1}, 1558 cm^{-1} and 1410 cm^{-1} were ascribed to bound water, N–H (amide II) stretching, and C–H bending of $–CH_2$, respectively [37]. The bands appearing from 920 cm^{-1} to 1039 cm^{-1} were due to C–O–C stretching [38]. After incorporation of TiO_2-N, partial peak intensities changed, but no noticeable wavenumber shift or peak appeared, or disappeared, which showed that only the possible formation of physical interaction occurred between the nanofiller and the biopolymer matrix. Similar results pertaining to the interaction of a bio-polymer matrix with other nanoparticles have been reported [21,39,40]. However, small modifications were found in the spectra after addition of CO. The peaks at 3420 cm^{-1}, 1558 cm^{-1}, 1410 cm^{-1} and 1039 cm^{-1} became sharper. Moreover, new peaks appeared at 2310 cm^{-1} and 996 cm^{-1}, which were assigned to residual CO_2 from atmosphere and C–O–C vibrations. This result indicated that incorporation of CO in the film could cause some interactions (such as hydrogen bonding or covalent bonding) between CO and the film matrix.

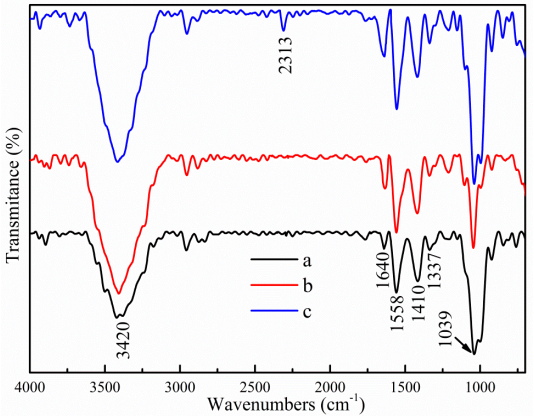

Figure 1. FTIR spectra of different samples. (**a**) Control; (**b**) 3% TiO_2-N; and (**c**) 9% CO-3% TiO_2-N.

3.1.2. Microstructure

SEM images of cross-sections of different samples are shown in Figure 2. The structure of the specimens was influenced by the presence or absence of TiO_2-N and CO. The control film displayed a smooth, compact, continuous structure without cracks or pores. The addition of TiO_2-N caused slight changes in the film structure, and some granules were present in the film. The number of granules was increased in the film structures with increasing TiO_2-N concentration, however after incorporation of CO the structure became heterogeneous. As the CO content increased, the roughness of the cross-section of films was increased. The CO droplets were well embedded in the film matrix, and the number and size thereof increased with increasing CO content. The phenomenon showed the existence of CO on the structure of the film. Moreover, no evidence was observed that CO droplets were separated from the film matrix network, which indicated that CO was well emulsified and dispersed in the film matrix. The results were similar to those of Peng et al. [41].

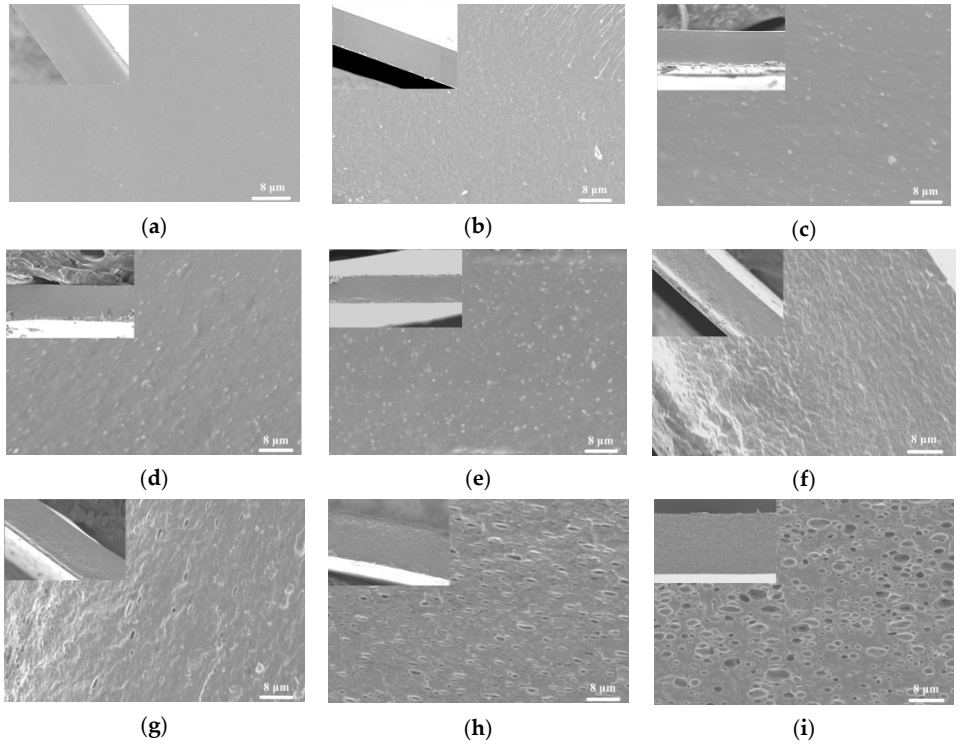

Figure 2. SEM micrographs of cross sections of films. (**a**) Control; (**b**) 1% TiO_2-N; (**c**) 3% TiO_2-N; (**d**) 5% TiO_2-N; (**e**) 7% TiO_2-N; (**f**) 3% CO-3% TiO_2-N; (**g**) 6% CO-3% TiO_2-N; (**h**) 9% CO-3% TiO_2-N; and (**i**) 12% CO-3% TiO_2-N.

3.1.3. Thermal Stability

To evaluate the effect of TiO_2-N and CO addition on the thermal stability of such films, TGA experiments were undertaken. The TG and DTG curves of different films are illustrated in Figure 3. Control film specimens displayed three stages in the process of thermal decomposition, ranging from 40–150 °C, 150–235 °C and 235–500 °C, ascribed to the evaporation of water and solvent, decomposition of lower molecular weight fractions, and pyrolytic decomposition of biopolymer chains, respectively. When 3% TiO_2-N was added to control film specimens, the TG curve of this sample showed a similar behaviour to that of the control sample, which indicated that the addition of TiO_2-N did not affect the thermal stability of the film.

As can be seen, four stages in the process of thermal decomposition were found in the film to which 3% TiO_2-N and 9% CO had been added. The top three stages of mass loss of the film were similar to those for the control film and 3% TiO_2-N film specimens. The fourth step took place between 380 and 460 °C and was attributed to decomposition of CO, which could be ascribed to the CO being stably embedded in the film network. Similar results were observed by Sliva [42] and Shen [43]. It was interesting to note that when 9% CO and 3% TiO_2-N were added to the control film, the mass loss below 420 °C was lower in comparison to control and 3% TiO_2-N films. This could be ascribed to the presence of CO, thus decreasing the moisture content of the sample. Moreover, as can be seen from the curves, the thermal degradation temperatures of the film were slightly increased after addition of 9% CO, which suggested that CO could increase the thermal stability of such films.

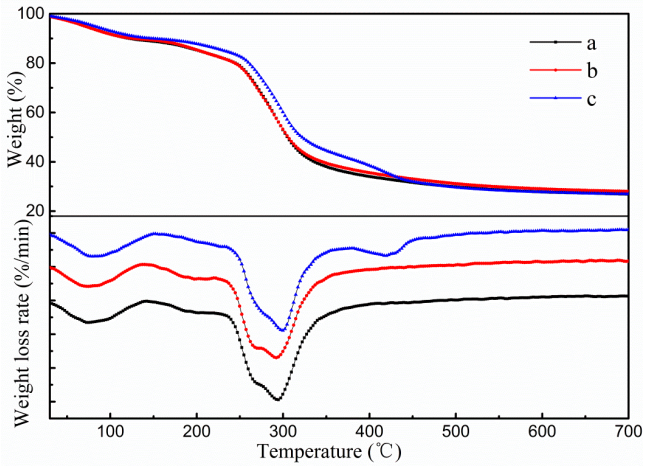

Figure 3. TG–DTG graphs of different samples. (**a**) Control; (**b**) 3% TiO_2-N; and (**c**) 9% CO-3% TiO_2-N.

3.1.4. Morphology Analysis

Figure 4 shows the morphology of different samples. The control film had a transparent and colourless form, however the addition of TiO_2-N caused obvious differences in morphology: The colour changed from colourless to white and the transparency was lower. This was due to the dyeing effect of TiO_2-N. After addition of CO, the morphology of the film underwent no significant change, letters could be observed clearly through the film, which was probably due to the emulsification and dispersion of CO in the film network.

The prepared film was flexible and glossy (Figure 4d). The morphology suggested that CO could increase the pliability of the sample, which could be attributed to interactions between the film matrix and CO. The result indicated that a continuous and flexible film material could be obtained based on CH, ST, TiO_2-N and CO by solution casting.

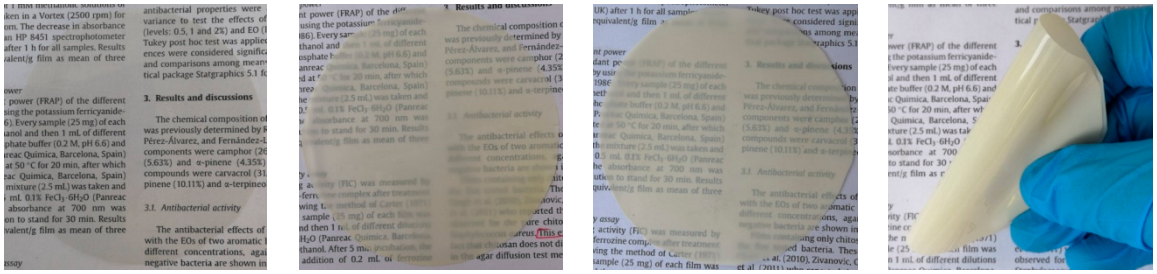

(**a**) (**b**) (**c**) (**d**)

Figure 4. Appearance of different films. (**a**) Control; (**b**) 3% TiO_2-N; and (**c**,**d**) 9% CO-3% TiO_2-N.

3.2. Physico-Chemical Properties

3.2.1. Mechanical Properties

To evaluate the effect of TiO_2-N and CO addition on the mechanical properties of films, tensile tests were conducted; the values of tensile strength (TS) and elongation at break (EAB) for different films are listed in Table 1. A significant increase was observed in TS and EAB decreased upon incorporation of TiO_2-N. These changes could be ascribed to the interfacial interaction between TiO_2-N and bio-polymer matrix. Nanoparticles could form intermolecular hydrogen bonds or covalent bonds with the CH or ST, consequently strengthening the molecular forces between the nanoparticles and the film matrix [21,36]. It can be seen that the TS first increased rapidly when the amount of TiO_2-N increased from 0% (33.2 MPa) to 3% (39.2 MPa), but increased little thereafter. A decrease (from 21.3% to 18.9%) in EAB film was observed upon addition of 3% TiO_2-N, but the EAB decreased more at higher doses thereof.

As expected, the introduction of CO significantly changed the TS and EAB of the samples. The TS gradually decreased with increasing CO content: This decrease was possibly due to the weaker polymer–oil interactions partially replacing the stronger polymer–polymer interactions in the film, thus decreasing the cohesion conferred by polymer network forces. Besides, the presence of CO droplets in the film partially destroyed the continuous structure of the sample, however the EAB of samples increased with addition of CO and reached a maximum value at 30.8% when the CO content was 9%, but decreased at higher CO contents. These changes could be ascribed to the CO droplets enhancing the mobility and destroying the even structure of film (Shen et al. also found similar results [43]).

Table 1. Physical and mechanical properties.

Films	Thickness (mm)	TS (MPa)	EAB (%)	MC (%)	Contact Angle (°)
Control	0.065 ± 0.009 ^{a}	33.2 ± 1.65 ^{d}	21.3 ± 5.2 ^{d}	12.5 ± 0.12 ^{d}	90.5 ± 1.37 ^{a}
1% TiO_2	0.068 ± 0.007 ^{ab}	37.8 ± 1.59 ^{e}	20.2 ± 3.5 ^{cd}	11.4 ± 0.28 ^{cd}	103.2 ± 1.25 ^{b}
3% TiO_2	0.067 ± 0.007 ^{ab}	39.2 ± 1.21 ^{f}	18.9 ± 4.3 ^{c}	10.9 ± 0.20 ^{c}	106.7 ± 0.58 ^{c}
5% TiO_2	0.066 ± 0.008 ^{a}	39.4 ± 0.88 ^{f}	16.2 ± 3.8 ^{b}	10.0 ± 0.31 ^{bc}	108.8 ± 1.08 ^{d}
7% TiO_2	0.067 ± 0.008 ^{ab}	37.7 ± 2.11 ^{e}	13.1 ± 4.5 ^{a}	9.20 ± 0.09 ^{b}	109.8 ± 1.25 ^{de}
3% TiO_2–3% CO	0.068 ± 0.009 ^{ab}	34.8 ± 2.21 ^{de}	24.5 ± 3.8 ^{e}	10.2 ± 0.11 ^{bc}	108.2 ± 1.15 ^{d}
3% TiO_2–6% CO	0.070 ± 0.006 ^{b}	31.3 ± 2.32 ^{c}	28.9 ± 1.9 ^{f}	9.62 ± 0.14 ^{b}	111.4 ± 0.51 ^{e}
3% TiO_2–9% CO	0.071 ± 0.004 ^{b}	29.1 ± 1.82 ^{b}	30.8 ± 3.2 ^{g}	8.91 ± 0.18 ^{ab}	113.2 ± 0.92 ^{f}
3% TiO_2–12% CO	0.072 ± 0.004 ^{b}	26.3 ± 1.14 ^{a}	26.2 ± 2.8 ^{ef}	8.41 ± 0.16 ^{a}	114.0 ± 0.86 ^{f}

Different letters in the same column indicate significant differences among formulations ($p < 0.05$).

3.2.2. Moisture Content and Water Contact Angle

The common methods of determining the hydrophobicity of edible film are the measurement of water contact angle and moisture uptake. Moisture content (MC) and water contact angle of samples are shown in Table 1 and Figure 5. As the amounts of TiO_2-N and CO increased, the MC decreased and the contact angle increased. When 3% TiO_2-N and 12% CO were added to the control film, the MC decreased from 12.5% to 8.41% and the contact angle increased from 90.5° to 114°, which indicated

that the addition of TiO_2-N and CO could effectively improve the films' hydrophobicity and its tendency to absorb water decreased. The result was likely to have been attributable to the interactions between TiO_2-N, CO and the film matrix reducing the tendency of hydroxyl groups to interact with water, consequently leading to a more hydrophobic matrix. Others reported that incorporation of nanoparticles or essential oil onto films results in the formation of more hydrogen bonds in the nanoparticles, oil droplets and matrix, thus enhancing the hydrophobicity of the material [19,44].

(**a**) (**b**) (**c**)

Figure 5. Static contact angle graphs of different films. (**a**) Control; (**b**) 3% TiO_2-N; and (**c**) 9% CO-3% TiO_2-N.

3.2.3. Water Vapour Permeability

The results of WVP testing are displayed in Table 2. Significant decreases in WVP occurred after incorporation of TiO_2-N and CO. As the content of TiO_2-N increased, the WVP of samples decreased. When 7% TiO_2-N was added, the WVP decreased from 1.406×10^{-10} to 1.288×10^{-10} g·m^{-1}·Pa^{-1}·s^{-1}. The decrease in WVP could be ascribed to the nanoparticles being more water resistant than the bio-composite matrix, and infilling of these nanoparticles into the matrix could form a dense structure and may have introduced a more tortuous pathway through which the water molecules had to pass [18,19,44,45]. Likewise, the WVP was also gradually decreased as more CO was added: When 12% CO was added, the WVP decreased from 1.285×10^{-10} to 1.058×10^{-10} g·m^{-1}·Pa^{-1}·s^{-1}, which suggested that the barrier-effect was improved. The result could be ascribed to the intermolecular interactions between CO and the film matrix, which reduced the adsorption of water in the film.

Table 2. Water vapour permeability (WVP) and antimicrobial properties.

Films	WVP (10^{-10} g/Pa·m·s)	Inhibitory Zone (mm^2)	
		S. aureus	*E. coli*
Control	1.406 ± 0.008 ^{a}	-	-
1% TiO_2	1.300 ± 0.019 ^{b}	30 ± 1.04 ^{a}	23 ± 1.02 ^{a}
3% TiO_2	1.285 ± 0.027 ^{bc}	43 ± 2.77 ^{b}	29 ± 2.11 ^{b}
5% TiO_2	1.204 ± 0.014 ^{c}	49 ± 3.14 ^{c}	34 ± 2.15 ^{c}
7% TiO_2	1.144 ± 0.028 ^{cd}	54 ± 0.89 ^{d}	39 ± 1.73 ^{d}
3% TiO_2–3% CO	1.202 ± 0.121 ^{c}	45 ± 1.89 ^{bc}	32 ± 3.88 ^{bc}
3% TiO_2–6% CO	1.154 ± 0.098 ^{cd}	48 ± 2.07 ^{c}	34 ± 1.17 ^{c}
3% TiO_2–9% CO	1.123 ± 0.201 ^{cd}	50 ± 3.55 ^{cd}	37 ± 2.04 ^{cd}
3% TiO_2–12% CO	1.058 ± 0.109 ^{d}	53 ± 3.73 ^{d}	40 ± 3.21 ^{d}

Different letters in the same column indicate significant differences among formulations ($p < 0.05$).

3.2.4. Colour Difference and Opacity

The colour characteristic parameters and light transmittance of different films are summarised in Table 3 and Figure 6. The values of L^*, WI and opacity were significantly increased as the content of TiO_2-N increased, which suggested that the brightness of films was affected by the addition of TiO_2-N: This could be attributed to the brightening effect of TiO_2-N. When CO was incorporated, L^* and WI decreased and a^* and b^* increased, which implied that the film had a lower lightness and

higher red and blue shades, which was due to the surface plasma resonance characteristics of TiO_2-N and coloured substances present in CO and its compounds. Opacity measurements indicated that the opacity was unchanged, which could be due to the CO droplets being well emulsified in the film.

Table 3. Colour difference and opacity.

Films	*L**	*a**	*b**	WI	Opacity
Control	66.43 ± 0.09 ^{a}	4.69 ± 0.23 ^{a}	8.67 ± 0.51 ^{a}	65.01 ± 0.15 ^{a}	0.74 ± 0.12 ^{a}
1% TiO_2	78.29 ± 0.16 ^{a}	5.30 ± 0.09 ^{a}	13.86 ± 0.79 ^{b}	73.70 ± 0.12 ^{a}	9.02 ± 0.18 ^{b}
3% TiO_2	81.33 ± 0.24 ^{a}	5.96 ± 0.24 ^{a}	13.56 ± 0.84 ^{bc}	76.17 ± 0.29 ^{ab}	19.4 ± 0.11 ^{c}
5% TiO_2	82.36 ± 0.09 ^{a}	6.14 ± 0.10 ^{a}	12.65 ± 0.42 ^{bc}	77.44 ± 0.31 ^{b}	29.3 ± 0.24 ^{d}
7% TiO_2	83.11 ± 0.09 ^{a}	6.21 ± 0.53 ^{a}	12.44 ± 0.72 ^{bc}	78.12 ± 0.15 ^{b}	34.6 ± 0.37 ^{e}
3% TiO_2–3% CO	78.42 ±0.07 ^{a}	6.98 ± 0.12 ^{a}	16.47 ± 0.11 ^{c}	72.51 ± 0.14 ^{b}	22.4 ± 0.31 ^{c}
3% TiO_2–6% CO	77.77 ± 0.47 ^{a}	7.95 ± 0.18 ^{a}	17.72 ± 0.84 ^{bc}	70.48 ± 0.39 ^{ab}	24.4 ± 0.14 ^{cd}
3% TiO_2–9% CO	77.44 ± 0.17 ^{a}	8.68 ± 0.11 ^{a}	19.50 ± 0.14 ^{bc}	68.94 ± 0.42 ^{ab}	25.8 ± 0.22 ^{cd}
3% TiO_2–12% CO	77.24 ± 0.09 ^{a}	8.87 ± 0.36 ^{a}	19.52 ± 0.33 ^{b}	68.73 ± 0.45 ^{a}	26.9 ± 0.34 ^{cd}

Different letters in the same column indicate significant differences among formulations ($p < 0.05$).

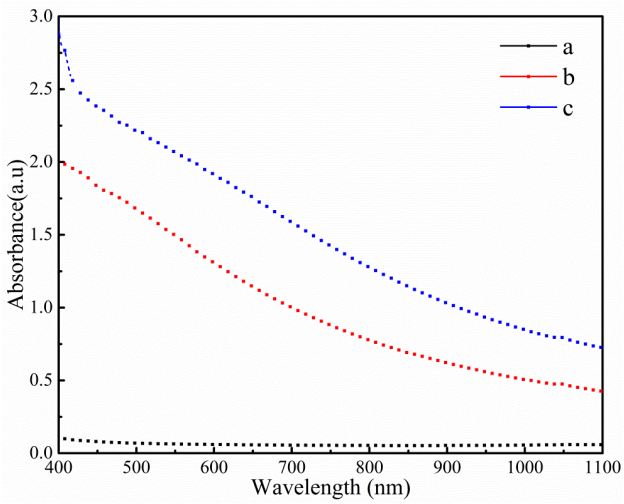

Figure 6. Visible absorbance for different films. (**a**) Control; (**b**) 3% TiO_2; and (**c**) 3% TiO_2–9% CO.

3.3. Biological Properties

3.3.1. Antimicrobial Activity

Table 2 showed the antimicrobial activities of the films. The control film showed no significant antimicrobial activity and revealed no obvious inhibition zones. This phenomenon could be ascribed to the fact that CH cannot diffuse through the adjacent agar media [46]. Many studies have indicated that there was good compatibility and hydrogen bond interaction between CH and ST molecules in the matrix [37,47]. Thus, CH molecules were supposed to be immobilised in the matrix and not diffused to generate an inhibition zone. As expected, the introduction of TiO_2-N significantly increased the inhibition zones of the two tested bacteria and the better inhibition of the samples was found with a higher TiO_2-N content. The effect could be ascribed to the nanoparticles having many unique effects, such as surface effects and small dimension effects, resulting in excellent biological and physico-chemical characteristics. A further increase in the size of the inhibition zones was observed when the CO was added. These results showed that the films dosed with TiO_2-N and CO could act as an antimicrobial material. The mechanism of the action thereof against microorganisms has been investigated elsewhere: The main antibacterial mechanism of TiO_2-N and CO was attributed

to an enhanced non-specific permeability of the cytoplasm membrane, leading to the bursting of cell membranes, thus killing the cell [12,34].

3.3.2. Antioxidant Activity

The DPPH radical scavenging activity of different samples is demonstrated in Figures 7 and 8. The control film had little scavenging activity (only 1.62%). Likewise, when TiO_2-N was added to the film, the scavenging activities were also under 2%, which indicated that TiO_2-N had not imparted any antioxidant activity. However, the scavenging activity of the sample increased significantly when CO was incorporated. Figure 8 shows that samples dosed with CO could act as stronger donors of electrons or hydrogen atoms to make the purple working solution fade to yellow [16]. The scavenging activities of the film were found to be around 1.78% (without CO), with the value increasing 13.2-, 16.1-, 25.4- and 29.3-fold in presence of 3%, 6%, 9% and 12% CO, respectively. This indicated that the scavenging activity of the samples was increased upon CO addition.

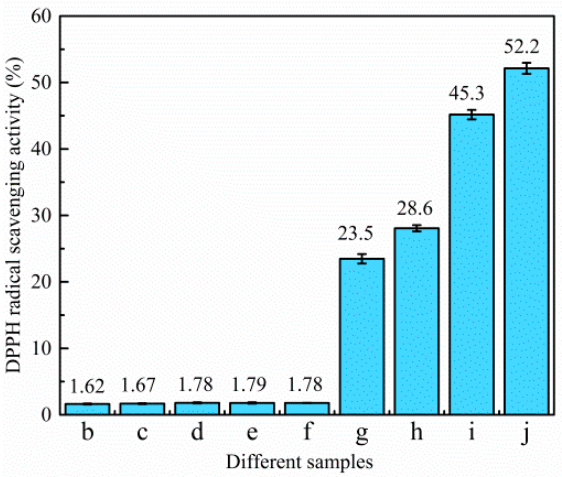

Figure 7. DPPH radical scavenging activity. (**b**) Control film; (**c**) 1% TiO_2-N; (**d**) 3% TiO_2-N; (**e**) 5% TiO_2-N; (**f**) 7% TiO_2-N; (**g**) 3% CO-3% TiO_2-N; (**h**) 6% CO-3% TiO_2-N; (**i**) 9% CO-3% TiO_2-N; and (**j**) 12% CO-3% TiO_2-N.

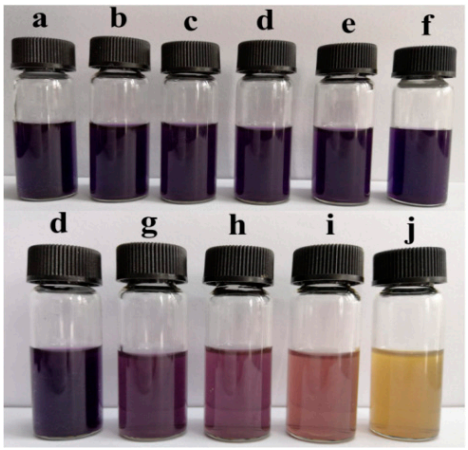

Figure 8. Pictures of DPPH radical scavenging activity. (**a**) DPPH methanol solution; (**b**) control film; (**c**) 1% TiO_2-N; (**d**) 3% TiO_2-N; (**e**) 5% TiO_2-N; (**f**) 7% TiO_2-N; (**g**) 3% CO-3% TiO_2-N; (**h**) 6% CO-3% TiO_2-N; (**i**) 9% CO-3% TiO_2-N; and (**j**) 12% CO-3% TiO_2-N.

The ABTS radical scavenging activity of different films is shown in Figures 9 and 10. The control film had a scavenging activity of 19.46%. After the addition of TiO_2-N, the scavenging activity decreased slightly, which could be attributed to the fact that TiO_2-N can act as a photocatalyst in the presence of water and generate reactive oxygen species; however, CO could improve the scavenging activity. When 12% CO was incorporated to the films, the scavenging activity increased from 16.53% to 44.72%. Figure 10 shows that samples with added CO could act as stronger donors of electrons or hydrogen atoms to fade the blue colour of the reaction solutions. The result showed that CO could enhance the antioxidant ability of such films.

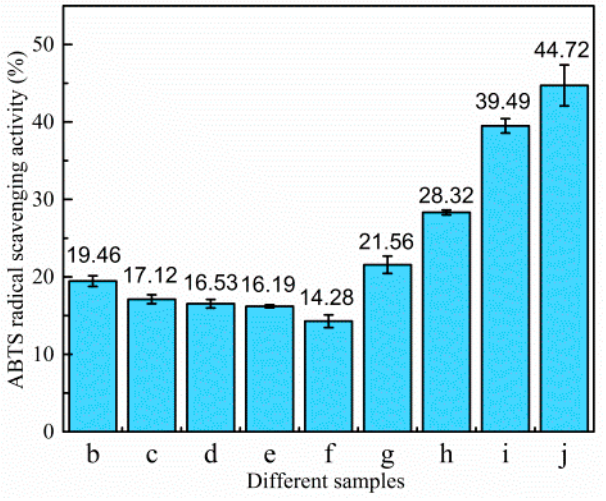

Figure 9. ABTS radical scavenging activity. (**b**) Control film; (**c**) 1% TiO_2-N; (**d**) 3% TiO_2-N; (**e**) 5% TiO_2-N; (**f**) 7% TiO_2-N; (**g**) 3% CO-3% TiO_2-N; (**h**) 6% CO-3% TiO_2-N; (**i**) 9% CO-3% TiO_2-N; and (**j**) 12% CO-3% TiO_2-N.

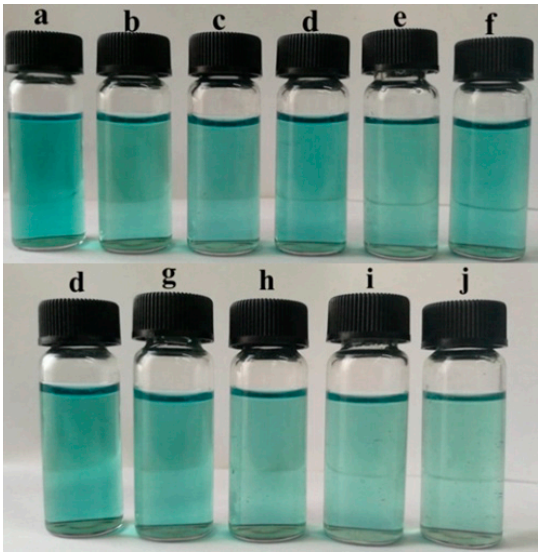

Figure 10. Pictures of ABTS radical scavenging activity. (**a**) ABTS solution; (**b**) control film; (**c**) 1% TiO_2-N; (**d**) 3% TiO_2-N; (**e**) 5% TiO_2-N; (**f**) 7% TiO_2-N; (**g**) 3% CO-3% TiO_2-N; (**h**) 6% CO-3% TiO_2-N; (**i**) 9% CO-3% TiO_2-N; and (**j**) 12% CO-3% TiO_2-N.

4. Conclusions

In this work, TiO_2-N and CO were introduced to a CH/ST matrix to prepare a novel active edible film. With the addition of TiO_2-N, the physico-chemical and antimicrobial properties of the sample increased, but the transparency decreased which suggested that the density of the film had

been increased. Incorporation of CO in the films decreased TS but increased the hydrophobicity and biological properties. Results of this work indicated that a good compatibility could be obtained between TiO_2-N, CO and the film matrix. Structural characterisation showed that the intermolecular interactions and compatibility were prepared between appropriate proportions of TiO_2-N, CO and the film matrix. FTIR spectra showed that some interactions occurred between TiO_2-N, CO and the film matrix. SEM and TG indicated that TiO_2-N and CO were well-dispersed and emulsified in the film network. Active film prepared from TiO_2-N, CO, CH and ST has good physico-chemical and biological properties, and thus offered a potential formulation option for food preservation products.

Author Contributions: C.Q. and W.L. designed the experiments; K.Z. prepared the paper; and H.C.; S.F.; W.W. and S.F. performed the experiments.

Funding: This research was funded by the Science and Technology Department of Hubei Province of China (Grant Number 2018ACA152).

Acknowledgments: The authors are grateful for the Science and Technology Department of Hubei Province of China and give thanks to the Hubei Provincial Key Laboratory of Biomass Resources Chemistry and Environmental Biotechnology for supporting this project.

Conflicts of Interest: Authors declare no conflicts of interest.

Abbreviations

CH	chitosan
ST	starch
TiO_2-N	nano titanium dioxide
CO	clove oil

References

1. Elsabee, M.Z.; Abdou, E.S. Chitosan based edible films and coatings: A review. *Mater. Sci. Eng. C.* **2013**, *33*, 1819–1841. [CrossRef] [PubMed]
2. Dehghani, S.; Hosseini, S.V.; Regenstein, J.M. Edible films and coatings in seafood preservation: A review. *Food Chem.* **2018**, *240*, 505–513. [CrossRef] [PubMed]
3. Cazón, P.; Velazquez, G.; Ramírez, J.A.; Vázquez, M. Polysaccharide-based films and coatings for food packaging: A review. *Food Hydrocoll.* **2017**, *68*, 136–148. [CrossRef]
4. Chillo, S.; Flores, S.; Mastromatteo, M.; Conte, A.; Gerschenson, L.; Del Nobile, M.A. Influence of glycerol and chitosan on tapioca starch-based edible film properties. *Int. J. Food Eng.* **2008**, *88*, 159–168. [CrossRef]
5. Kerch, G. Chitosan films and coatings prevent losses of fresh fruit nutritional quality: A review. *Trends Food Sci. Technol.* **2015**, *46*, 159–166. [CrossRef]
6. Özdemir, K.S.; Gökmen, V. Extending the shelf-life of pomegranate arils with chitosan-ascorbic acid coating. *LWT Food Sci. Technol.* **2017**, *76*, 172–180. [CrossRef]
7. Zhao, Y.; Teixeira, J.S.; Gänzle, M.M.; Saldaña, M.D.A. Development of Antimicrobial Films Based on Cassava Starch, Chitosan and Gallic Acid Using Subcritical Water Technology. *J. Supercrit. Fluids* **2018**, *137*, 101–110. [CrossRef]
8. Pinzon, M.; Garcia, O.; Villa, C. The influence of Aloe vera gel incorporation on the physicochemical and mechanical properties of banana starch-chitosan edible films. *J. Sci. Food Agric.* **2018**, *98*, 4042–4049. [CrossRef]
9. Aider, M. Chitosan application for active bio-based films production and potential in the food industry: Review. *LWT Food Sci. Technol.* **2010**, *43*, 837–842. [CrossRef]
10. Schreiber, S.B.; Bozell, J.; Hayes, D.G.; Zivanovic, S. Introduction of primary antioxidant activity to chitosan for application as a multifunctional food packaging material. *Food Hydrocoll.* **2013**, *33*, 207–214. [CrossRef]
11. Rinaudo, M. Chitin and chitosan: Properties and applications. *Prog. Polym. Sci.* **2006**, *31*, 603–632. [CrossRef]
12. Ren, L.; Yan, X.; Zhou, J.; Tong, J.; Su, X. Influence of chitosan concentration on mechanical and barrier properties of corn starch/chitosan films. *Int. J. Biol. Macromol.* **2017**, *105*, 1636–1643. [CrossRef] [PubMed]
13. Bonila, J.; Atarés, L.; Varges, M.; Chiralt, A. Properties of wheat starch film-forming dispersions and films as affected by chitosan addition. *J. Food Eng.* **2013**, *114*, 303–312. [CrossRef]

14. Mohammadi, R.; Mohammadifar, M.A.; Rouhi, M.; Mohaddeseh, K.; Amir, M.M.; Ehsan, S.; Sara, H. Physico-mechanical and structural properties of eggshell membrane gelatin-chitosan blend edible films. *Int. J. Biol. Macromol.* **2017**, *107*, 406–412. [CrossRef] [PubMed]
15. Talón, E.; Trifkovic, K.T.; Nedovic, V.A.; Bugarski, B.M.; Vargas, M.; Chiralt, A.; González-Martínez, C. Antioxidant edible films based on chitosan and starch containing polyphenols from thyme extracts. *Carbohydr. Polym.* **2017**, *157*, 1153–1161. [CrossRef] [PubMed]
16. Pérez-Córdoba, L.J.; Norton, L.T.; Batchelor, H.K.; Gkatzionis, K.; Spyropoulos, F.; Sobral, P.J.A. Physico-chemical, antimicrobial and antioxidant properties of gelatin-chitosan based films loaded with nanoemulsions encapsulating active compounds. *Food Hydrocoll.* **2018**, *79*, 544–559. [CrossRef]
17. Yang, J.; Xiong, L.; Li, M.; Sun, Q.J. Chitosan–Sodium Phytate Films with a Strong Water Barrier and Antimicrobial Properties Produced via One-Step-Consecutive-Stripping and Layer-by-Layer-Casting Technologies. *J. Agric. Food Chem.* **2018**, *66*, 6104–6115. [CrossRef]
18. Sadegh-Hassani, F.; Nafchi, A.M. Preparation and characterization of bionanocomposite films based on potato starch/halloysite nanoclay. *Int. J. Biol. Macromol.* **2014**, *67*, 458–462. [CrossRef]
19. Akbariazam, M.; Ahmadi, M.; Javadian, N.; Nafchi, A.M. Fabrication and characterization of soluble soybean polysaccharide and nanorod-rich ZnO bionanocomposite. *Int. J. Biol. Macromol.* **2016**, *89*, 369–375. [CrossRef]
20. Yin, C.; Huang, C.X.; Wang, J.; Liu, Y.; Lu, P.; Huang, L.J. Effect of Chitosan- and Alginate-Based Coatings Enriched with Cinnamon Essential Oil Microcapsules to Improve the Postharvest Quality of Mangoes. *Materials* **2019**, *12*, 2039. [CrossRef]
21. Marvizadeh, M.M.; Oladzadabbasabadi, N.; Nafchi, A.M.; Jokar, M. Preparation and characterization of bionanocomposite film based on tapioca starch/bovine gelatin/nanorod zinc oxide. *Int. J. Biol. Macromol.* **2017**, *99*, 1–7. [CrossRef] [PubMed]
22. Abdollahi, M.; Rezaei, M.; Farzi, G. A novel active bionanocomposite film incorporating rosemary essential oil and nanoclay into chitosan. *J. Food Eng.* **2012**, *111*, 343–350. [CrossRef]
23. Mei, J.; Yuan, Y.; Guo, Q.; Wu, Y.; Li, Y.; Yu, H. Characterization and antimicrobial properties of water chestnut starch-chitosan edible films. *Int. J. Biol. Macromol.* **2013**, *61*, 169–174. [CrossRef] [PubMed]
24. Altln, I.; Sökmen, M. Preparation of TiO_2-polystyrene photocatalyst from waste material and its usability for removal of various pollutants. *Appl. Catal. B Environ.* **2014**, *144*, 694–701.
25. Zhang, X.; Xiao, G.; Wang, Y.; Zhao, Y.; Su, H.; Tan, T. Preparation of chitosan-TiO_2 composite film with efficient antimicrobial activities under visible light for food packaging applications. *Carbohydr. Polym.* **2017**, *169*, 101–107. [CrossRef] [PubMed]
26. He, Q.; Huang, Y.; Lin, B.; Wang, S. A nanocomposite film fabricated with simultaneously extracted protein-polysaccharide from a marine alga and TiO2nanoparticles. *J. Appl. Phycol.* **2017**, *29*, 1541–1552. [CrossRef]
27. Zheng, K.; Xiao, S.; Li, W.; Wang, W.; Chen, H.; Yang, F.; Qin, C. Chitosan-acorn starch-eugenol edible film: Physico-chemical, barrier, antimicrobial, antioxidant and structural properties. *Int. J. Biol. Macromol.* **2019**, *135*, 344–352. [CrossRef]
28. Alparslan, Y. Antimicrobial and antioxidant capacity of biodegradable gelatin film forming solutions incorporated with different essential oils. *J. Food Meas. Charact.* **2018**, *12*, 317–322. [CrossRef]
29. EI-Mesallamy, A.M.D.; EI-Gerby, M.; Azim, M.H.A.E.; Awad, A. Antioxidant, Antimicrobial Activities and Volatile Constituents of Clove Flower Buds Oil. *J. Essent. Oil Bear. Plants* **2012**, *15*, 900–907. [CrossRef]
30. Aguilar-Sánchez, R.; Munguía-Pérez, R.; Reyes-Jurado, F.; Navarro-Cruz, A.R.; Cid-Pérez, T.S.; Hernández-Carranza, P.; Beristain-Bauza, S.C.; Ochoa-Velasco, C.E.; Avila-Sosa, R. Structural, Physical, and Antifungal Characterization of Starch Edible Films Added with Nanocomposites and Mexican Oregano (Lippia berlandieri Schauer) Essential Oil. *Molecules* **2019**, *24*, 2340. [CrossRef]
31. Wu, J.; Sun, Q.; Huang, H.; Duan, Y.; Xiao, G.; Le, T. Enhanced physico-mechanical, barrier and antifungal properties of soy protein isolate film by incorporating both plant-sourced cinnamaldehyde and facile synthesized zinc oxide nanosheets. *Colloids Surf. B Biointerfaces* **2019**, *180*, 31–38. [CrossRef] [PubMed]
32. Wu, Z.; Zhou, W.; Pang, C.; Deng, W.; Xu, C.; Wang, X. Multifunctional chitosan-based coating with liposomes containing laurel essential oils and nanosilver for pork preservation. *Food Chem.* **2019**, *295*, 16–25. [CrossRef] [PubMed]
33. Nafchi, A.M.; Moradpour, M.; Saeidi, M.; Alias, A.K. Thermoplastic starches: Properties, challenges, and prospects. *Starch Stärke* **2013**, *65*, 61–72. [CrossRef]

34. Nafchi, A.M.; Alias, A.K.; Muhmud, S.; Robal, M. Antimicrobial, rheological, and physicochemical properties of sago starch films filled with nanorod-rich zinc oxide. *J. Food Eng.* **2012**, *113*, 511–519. [CrossRef]
35. Zheng, L.; Zhao, M.; Xiao, C.; Zhao, Q.; Su, G. Practical problems when using ABTS assay to assess the radical-scavenging activity of peptides: Importance of controlling reaction pH and time. *Food Chem.* **2016**, *192*, 288–294. [CrossRef] [PubMed]
36. Rezaei, M.; Ojagh, S.M.; Razavi, S.H.; Hosseini, S.M.H. Development and evaluation of a novel biodegradable film made from chitosan and cinnamon essential oil with low affinity toward water. *Food Chem.* **2010**, *122*, 161–166. [CrossRef]
37. Silva-Pereira, M.C.; Teixeira, J.A.; Pereira-Júnior, V.A.; Stefani, R. Chitosan/corn starch blend films with extract from Brassica oleraceae (red cabbage) as a visual indicator of fish deterioration. *LWT Food Sci. Technol.* **2015**, *61*, 258–262. [CrossRef]
38. Namazi, H.; Dadkhah, A. Convenient method for preparation of hydrophobically modified starch nanocrystals with using fatty acids. *Carbohydr. Polym.* **2010**, *79*, 731–737. [CrossRef]
39. Nafchi, A.M.; Moradpour, M.; Saeidi, M.; Alias, A.K. Effects of nanorod-rich ZnO on rheological, sorption isotherm, and physicochemical properties of bovine gelatin films. *LWT Food Sci. Technol.* **2014**, *58*, 142–149. [CrossRef]
40. Nafchi, A.M.; Nassiri, R.; Sheibani, S.; Ariffin, F.; Karim, A.A. Preparation and characterization of bionanocomposite films filled with nanorod-rich zinc oxide. *Carbohydr. Polym.* **2013**, *96*, 233–239. [CrossRef] [PubMed]
41. Peng, Y.; Li, Y. Combined effects of two kinds of essential oils on physical, mechanical and structural properties of chitosan films. *Food Hydrocoll.* **2014**, *36*, 287–293. [CrossRef]
42. Silva, M.F.; Lopes, P.S.; Silva, C.F.; Yoshida, C.M.P. Active packaging material based on buriti oil—Mauritia flexuosa L.f. (Arecaceae) incorporated into chitosan films. *J. App. Polym. Sci.* **2016**, *133*, 43210–43218.
43. Shen, Z.; Kamdem, D.P. Development and characterization of biodegradable chitosan films containing two essential oils. *Int. J. Biol. Macromol.* **2015**, *74*, 289–296. [CrossRef] [PubMed]
44. Teymourpour, S.; Nafchi, A.M.; Nahidi, F. Functional, thermal, and antimicrobial properties of soluble soybean polysaccharide biocomposites reinforced by nano TiO_2. *Carbohydr. Polym.* **2015**, *134*, 726–731.
45. Tongnuanchan, P.; Benjakul, S.; Prodpran, T. Moreover, the presence of CO droplets increased the distance travelled by water molecules diffusing through the film matrix. *Food Chem.* **2012**, *134*, 1571–1579. [CrossRef] [PubMed]
46. Valodkar, M.; Thakore, S. Isocyanate crosslinked reactive starch nanoparticles for thermo-responsive conducting applications. *Carbohydr. Res.* **2010**, *345*, 2354–2360. [CrossRef] [PubMed]
47. Zhang, L.; Jiang, Y.; Ding, Y.; Daskalakis, N. Mechanistic investigation into antibacterial behaviour of suspensions of ZnO nanoparticles against *E. coli*. *J. Nanopart. Res.* **2010**, *12*, 1625–1636. [CrossRef]